J. Fluid Mech. (1992), *vol.* 244, *pp.* 615–632

Fluid-elastic instabilities of liquid-lined flexible tubes

By D. HALPERN AND J. B. GROTBERG

Biomedical Engineering Department, Robert R. McCormick School of Engineering and Applied Science Northwestern University, Evanston, IL 60208, USA *and* Department of Anesthesia, Northwestern University Medical School, Chicago, IL 60611, USA

(Received 28 February 1991 and in revised form 16 December 1991)

The dynamics of a thin film of Newtonian fluid coating the inner surface of an elastic circular tube is analysed. This problem is motivated by an interest in the closure of small airways of the lungs either by formation of a liquid bridge, the collapse of the airway wall or a combination of both processes. Liquid bridge formation is due to the destabilization of the liquid film that coats the inner surface of airways, while wall collapse can be due to either the high surface tension of the air–liquid interface or the flexibility of the wall.

Nonlinear evolution equations for the film thickness and wall position are derived using lubrication theory, but an accurate representation of the curvatures of both the liquid and wall interfaces is employed which is valid for thick films. These approximations allow closure to be predicted. In addition, these approximations are justified by comparison with rigid-wall results obtained by solving the full Navier–Stokes equations and because fluid inertia only becomes important in the very late stages of closure. The linear stability of these equations is examined using normal-mode analysis for infinitesimal disturbances and the nonlinear stability is investigated by solving the governing equations numerically using the method of lines. Solutions show that there is a critical film thickness, strongly dependent on fluid and wall properties, above which unstable waves grow to form liquid bridges. The critical film thickness decreases with increasing surface tension or wall compliance since waves grow faster. Even for relatively stiff airways, the volume of fluid in the liquid lining required for closure can be approximately 70% of the volume for the rigid-tube case. Wall damping is an important effect only when the airway is sufficiently compliant. Airway closure occurs more rapidly with increasing unperturbed film thickness, surface tension and wall flexibility and decreasing wall damping.

1. Introduction

It is well recognized that the thin liquid film which lines the inner surface of the lungs' airways may cause closing off of the small airways in the region of the respiratory bronchioles either by the formation of a meniscus or by provoking collapse of the flexible wall of such airways (Macklem, Proctor & Hogg 1970). This happens most frequently near the end of expiration when the airway diameters are small (Hughes, Rosenzweig & Kivitz 1970; Kamm & Schroter 1989). The closure and subsequent reopening of these airways contributes to the shape of the pressure–volume curve in cycled lungs, since the capacity to accommodate air volume is cyclically enhanced and disenhanced when the alveolar regions distal to the sites

of closure are recruited and de-recruited (Frazer, Weber & Franz 1985). The shape of this curve characterizes the mechanical response of the lung. Measuring the occurrence of airway closure is one component of a standard pulmonary function test: the single-breath nitrogen washout test. When this test shows early airway closure, it is often interpreted that there is inhomogeneous ventilation distribution within the lung, which may be caused by a number of normal and pathological conditions (Crawford *et al.* 1989). Since diseases of the small airways are difficult to detect, especially at an early stage, results of this test carry particular significance.

The dynamic stability of a thin liquid film has been investigated by Goren (1962), Hickox (1971), Hammond (1983), Gauglitz & Radke (1988), Kamm & Johnson (1990) and Johnson *et al.* (1991). Hammond (1983) and Gauglitz & Radke (1988) were both interested in engineering applications such as two-phase flows in porous media, where one fluid displaces another, and a thin film of fluid is left behind wetting the walls of the conduit. Kamm & Johnson (1990) and Johnson *et al.* (1991) included the effects of fluid inertia in a one-dimensional model to simulate airway closure at low lung volumes. In addition, Otis *et al.* (1990) included the effects of surfactant on the surface tension of the interface. Further aspects which may be relevant to the lungs are the viscoelastic properties of the liquid lining and the airways. In this paper we will investigate the effects of airway flexibility but assume a constant interfacial surface tension and a Newtonian fluid.

Nonlinear evolution equations for the film thickness and the wall position are derived using lubrication theory since the film coating the wall is extremely thin and the Reynolds number is at most $O(1)$. Hammond's (1983) thin-film analysis showed that initial sinusoidal disturbances with wavelengths greater than the circumference of the inviscid core evolve into stable wetting collars of constant mean curvature, with dry patches between collars under certain conditions. However, meniscus formation was not predicted. Gauglitz & Radke (1988) also employed a small-slope approximation but included a form of the Young–Laplace equation for the curvature of the film interface that is more accurate for thicker films. In addition, they used the axisymmetric form of the kinematic boundary condition which yields the evolution equation for the film thickness, instead of the two-dimensional form of the kinematic boundary condition used by Hammond (1983) which is asymptotically valid for thin films. They demonstrated numerically that meniscus formation occurs above a critical film thickness. Below this thickness, stable collars were obtained, as in Hammond (1983). This extension of Hammond's analysis is beyond the range of asymptotic validity when the film thickness becomes large. It has also been applied to other problems, where the physics is quite different, such as the Rayleigh–Taylor instability at a perturbed interface between two viscous fluid layers whose base flow is either Poiseuille or Couette flow, and the stability of flow down a vertical cylindrical surface (Oron & Rosenau 1989; Rosenau & Oron 1989). Johnson *et al.* (1991) used a model similar to that of Gauglitz & Radke (1988) to simulate airway closure except that they included fluid inertia in an *ad hoc* fashion. Their results agreed very well with solutions to the full problem for small Reynolds numbers and thicknesses outside the range of validity of lubrication theory. We will apply the model due to Gauglitz & Radke (1988) and show how the wall properties of a flexible elastic wall modify the stability results of Hammond (1983) and Gauglitz & Radke (1988).

In §2, the nonlinear dynamic model is formulated from first principles. Nonlinear evolution equations are derived in §3 for the film thickness and the tube using the lubrication theory approximation for long waves. These equations are first linearized

and their stability is investigated by the method of normal modes in §4. Numerical solutions to the full nonlinear problem are presented in §5 and the conclusions in §6.

2. Formulation of nonlinear model

2.1. *Fluid mechanics of the thin film*

Consider a core of Newtonian fluid of undisturbed radius b and viscosity $\lambda\mu$, surrounded by a thin film consisting of a different fluid of viscosity μ coating the inner surface of a flexible tube with an undisturbed radius a (figure 1). The dynamics of the core is neglected since we assume that $\lambda \ll 1$ and $H\lambda/a \ll 1$, where H is a characteristic film thickness (Hammond 1983). Consequently the pressure in the core is constant. The flow in the film can be modelled using continuity and Navier–Stokes equations which are given below:

$$\left.\begin{aligned} \nabla\cdot\boldsymbol{u}^* &= 0 \qquad (2.1a)\\ \rho\left(\frac{\partial \boldsymbol{u}^*}{\partial t^*}+\boldsymbol{u}^*\cdot\nabla\boldsymbol{u}^*\right) &= -\nabla p^*+\mu\nabla^2\boldsymbol{u}^* \qquad (2.1b)\end{aligned}\right\} \quad \text{for} \quad b+h^*(z^*,t^*) \leqslant r^* \leqslant a+\eta^*(z^*,t^*),$$

where $\boldsymbol{u}^*, p^*$ are the velocity vector and the pressure distribution in the film, respectively. The air–liquid interface is located at $r^* = b+h^*(z^*,t^*)$ and the tube wall at $r^* = a+\eta^*(z^*,t^*)$, where h^* and η^* are the respective axisymmetric deflections of the air–liquid and wall–liquid interfaces from their unperturbed states, and (r^*,θ,z^*) are the usual cylindrical coordinates. Axial wall deflection is not included since the tube is assumed to be tethered and only long-wavelength disturbances will be considered (Dragon & Grotberg 1991).

The kinematic boundary conditions at the liquid–wall interface are given by

$$u^* = \frac{\partial \eta^*}{\partial t^*}+w^*\left(\frac{\partial \eta^*}{\partial z^*}\right) \quad \text{and} \quad w^* = 0 \quad \text{at} \quad r^* = a+\eta^*(z^*,t^*), \quad (2.2a, b)$$

where u^* and w^* are the radial and axial components of velocity in the thin film.

Unit vectors tangential and normal to the air–liquid interface are given by

$$\hat{\boldsymbol{t}} = \left(1+\left(\frac{\partial h^*}{\partial z^*}\right)^2\right)^{-\frac{1}{2}}\left(\hat{\boldsymbol{z}}+\left(\frac{\partial h^*}{\partial z^*}\right)\hat{\boldsymbol{r}}\right) \qquad (2.3)$$

and

$$\hat{\boldsymbol{n}} = \left(1+\left(\frac{\partial h^*}{\partial z^*}\right)^2\right)^{-\frac{1}{2}}\left(\hat{\boldsymbol{r}}-\left(\frac{\partial h^*}{\partial z^*}\right)\hat{\boldsymbol{z}}\right), \qquad (2.4)$$

where $\hat{\boldsymbol{z}}$ and $\hat{\boldsymbol{r}}$ are the unit vectors in the axial and radial directions. Unit vectors $\hat{\boldsymbol{z}}_w$, $\hat{\boldsymbol{r}}_w$, $\hat{\boldsymbol{t}}_w$ and $\hat{\boldsymbol{n}}_w$ are defined similarly at the liquid–wall interface with h^* replaced by η^*. The tangential and normal stress conditions due to constant surface tension, σ, can be written in tensor form

$$\boldsymbol{T}^*\cdot\hat{\boldsymbol{n}} = \sigma\kappa^*\hat{\boldsymbol{n}} \qquad (2.5)$$

where the stress tensor for the film, $\boldsymbol{T}^*$, is given by

$$\boldsymbol{T}^* = -p^*\boldsymbol{I}+\mu(\nabla\boldsymbol{u}^*+\nabla\boldsymbol{u}^{*\mathrm{T}}) \qquad (2.6)$$

and κ^* is the curvature of the interface:

$$\kappa^* = \nabla\cdot\hat{\boldsymbol{n}} = \frac{1}{b+h^*}\left(1+\left(\frac{\partial h^*}{\partial z^*}\right)^2\right)^{-\frac{1}{2}}-\frac{\partial^2 h^*}{\partial z^{*2}}\left(1+\left(\frac{\partial h^*}{\partial z^*}\right)^2\right)^{-\frac{3}{2}}. \qquad (2.7)$$

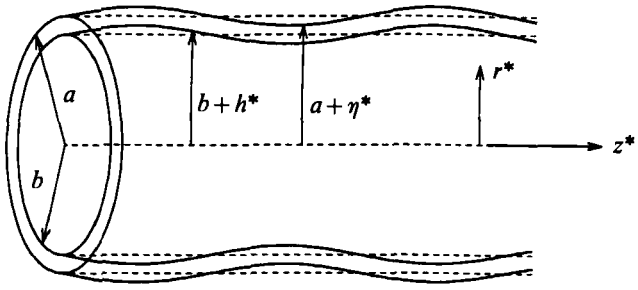

FIGURE 1. Variables describing geometry of air–liquid and wall–liquid interfaces.

Since the air–liquid interface is a material surface, we have the following kinematic boundary condition:

$$\frac{\partial h^*}{\partial t^*}+w^*\frac{\partial h^*}{\partial z^*}=u^* \quad \text{at} \quad r^*=b+h^*, \tag{2.8}$$

which can be written in terms of the axial flow rate, Q_w^*,

$$\frac{\partial h^*}{\partial t^*}=\frac{1}{b+h^*}\left((a+\eta^*)\frac{\partial \eta^*}{\partial t^*}+\frac{1}{2\pi}\frac{\partial Q_w^*}{\partial z^*}\right), \tag{2.9}$$

where

$$Q_w^*=2\pi\int_{b+h^*}^{a+\eta^*} w^* r^*\,\mathrm{d}r^*. \tag{2.10}$$

2.2. *Equation of motion of the tube*

The tube is assumed to be infinitely long, thin-walled, isotropic and impermeable. The relevant characteristics of the tube are its density ρ_w, modulus of elasticity E, damping coefficient g, longitudinal tension T_ℓ^*, circumferential tension, T_θ^*, thickness h_0 and Poisson ratio γ.

In the long-wavelength limit, axial deflections are much smaller than radial deflections (Atabek & Lew 1966; Dragon & Grotberg 1991). Consequently, we only consider normal forces acting at the liquid–wall interface. The equation of equilibrium of normal forces is given by

$$\rho_w h_0 g\frac{\partial \eta^*}{\partial t^*}\boldsymbol{r}_{\hat{w}}\cdot\boldsymbol{n}_{\hat{w}}+\frac{T_\theta^*}{a+\eta^*}\left(1+\left(\frac{\partial \eta^*}{\partial z^*}\right)^2\right)^{-\frac{1}{2}}-T_\ell^*\frac{\partial^2 \eta^*}{\partial z^{*2}}\left(1+\left(\frac{\partial \eta^*}{\partial z^*}\right)^2\right)^{-\frac{3}{2}}=-\boldsymbol{n}_{\hat{w}}\cdot\boldsymbol{T}^*\cdot\boldsymbol{n}_{\hat{w}}. \tag{2.11}$$

Wall inertia is negligible as is the fluid inertia in this problem. The circumferential tension, T_θ^*, is related to the radial strain in the following way (Goldenveizer 1961; Atabek & Lew 1966):

$$T_\theta^*=T_0^*+\frac{Eh_0}{1-\gamma^2}\frac{a\epsilon_\theta}{a+\eta^*}, \tag{2.12}$$

where T_0^* is the initial tension, and the strain assumes the following nonlinear law (Elad, Foux & Kivity 1988*a*):

$$\epsilon_\theta=\frac{1}{n}\left[\left(\frac{a+\eta^*}{a}\right)^n-1\right], \tag{2.13}$$

where $n\geqslant 1$.

3. Lubrication theory

Applying the lubrication theory approximation for thin films to the governing equations derived in §2.1, all lengthscales are non-dimensionalized with respect to the unperturbed tube radius a:

$$(h^*, \eta^*, r^*, z^*) = a(\epsilon h, \epsilon\eta, r, z) \tag{3.1}$$

and a new independent variable y is defined such that

$$r^* = a(1+\epsilon\eta-\epsilon y) \quad \text{where} \quad \epsilon = 1-b/a \ll 1 \tag{3.2}$$

so that $y = Y \equiv 1+\eta-h$ is the air–liquid interface and $y = 0$ is the wall–liquid interface. Following Hammond (1983), the velocity components, pressure distribution and time are scaled as follows:

$$u^* = \epsilon^4 \frac{\sigma}{\mu} u, \quad w^* = \epsilon^3 \frac{\sigma}{\mu} w, \quad p^* = \epsilon \frac{\sigma}{a} p, \quad t^* = \frac{\mu a}{\sigma} \epsilon^{-3} t. \tag{3.3}$$

Then the momentum equations in the thin film, (2.1b), become to leading order in ϵ,

$$\frac{\partial p}{\partial z} = \frac{\partial^2 w}{\partial y^2} + O(\epsilon^2, \epsilon^2 Re) \quad \text{and} \quad \frac{\partial p}{\partial y} = O(\epsilon^2, \epsilon^4 Re), \tag{3.4a, b}$$

where $Re = \epsilon^3 \rho\sigma a/\mu^2$ is the Reynolds number. Hence the fluid inertia terms can be neglected provided $\epsilon^2 Re \ll 1$. The boundary conditions at the liquid–wall interface, (2.2), are

$$u = \frac{\partial \eta}{\partial t} \quad \text{at} \quad y = 0 \quad \text{and} \quad w = 0, \tag{3.5a, b}$$

and the tangential and normal stress conditions at the air–liquid interface, (2.5), reduce to

$$\frac{\partial w}{\partial y} = 0 \quad \text{and} \quad p - p_{\text{core}} = \frac{\partial^2 h}{\partial z^2} - \frac{\epsilon^{-1}}{1+\epsilon(h-1)} \quad \text{at} \quad y = Y, \tag{3.6a, b}$$

where p_{core} is the constant pressure of the core, $p_{\text{core}} = 1/\epsilon(1-\epsilon)$, obtained by setting $h = 0$. Even though equation (3.6b) is asymptotically equivalent to $p = h_{zz} + h + O(\epsilon)$, by retaining some higher-order terms in the expressions for the principal radii of curvature it is possible to predict meniscus formation (Gauglitz & Radke 1988). This procedure of keeping selected higher terms has been applied to different problems and is often known as 'regularization'. For example, Oron & Rosenau (1989) derived a 'regularized' Kuramoto–Sivashinsky equation by applying an asymptotic approach which took into account large gradients and used the full expression for the curvature so that wave breaking could be observed. We could have used the exact expression for the curvature as given by (2.7) but Gauglitz & Radke (1988) demonstrated, by calculating the static shape of an interface that has constant mean curvature due to a uniform pressure difference, that (3.6b) is a good approximation to (2.7) in predicting what the maximum volume and radius of the liquid collar are before the formation of a meniscus.

If $\epsilon^2 Re \ll 1$, the pressure is independent of y and the longitudinal velocity, w, is determined by integrating the axial momentum equation, (3.4a), twice,

$$w = \frac{1}{2} \frac{\partial p}{\partial z} (y^2 - 2yY). \tag{3.7}$$

The pressure gradient is obtained by differentiating (3.6*b*). In the lubrication theory limit, Q_w^* is given by

$$Q_w^* = 2\pi\epsilon^4 \frac{a^2\sigma}{\mu} \int_0^Y w\,\mathrm{d}y + O(\epsilon^5). \tag{3.8}$$

A nonlinear evolution equation for h is obtained by substituting (3.6)–(3.8) into (2.9):

$$\frac{\partial h}{\partial t} = \frac{1}{1+\epsilon(h-1)}\left[(1+\epsilon\eta)\frac{\partial \eta}{\partial t} - \frac{1}{3}\frac{\partial}{\partial z}\left\{(1+\eta-h)^3\left(\frac{\partial^3 h}{\partial z^3} + \frac{1}{(1+\epsilon(h-1))^2}\frac{\partial h}{\partial z}\right)\right\}\right]. \tag{3.9}$$

In this small-slope approximation, due to Gauglitz & Radke (1988), the dependence on the circumferential film curvature, $1/1+\epsilon(h-1)$, is kept. Johnson *et al.* (1991) showed that this approximation works very well for rigid tubes ($E \to \infty$, $\eta = 0$) by comparing this type of model with numerical solutions to the full governing equations and boundary conditions.

The scalings used in the lubrication approximation are also applied to the wall equation. By applying the same approximation to the wall curvature in (2.11) as in (3.6) and using the scalings introduced in (3.1) and assuming a linear hoop stress law in (2.12), i.e. $n = 1$ in (2.13), equation (2.11) reduces to

$$p - p_{\text{ext}} = \epsilon^{-1}\frac{T_0}{1+\epsilon\eta} + \frac{1}{\Gamma}\frac{\eta}{(1+\epsilon\eta)^2} - T_\ell\frac{\partial^2\eta}{\partial z^2} + \epsilon^3 MG\frac{\partial \eta}{\partial t}, \tag{3.10}$$

where p_{ext} is the constant pressure outside the tube, $p_{\text{ext}} = -T_0/\epsilon$, and

$$\Gamma = \frac{(1-\gamma^2)\sigma}{Eh_0}, \quad T_\ell = \frac{T_\ell^*}{\sigma}, \quad T_0 = \frac{T_0^*}{\sigma}, \quad M = \frac{\rho_w h_0}{\rho a} \quad \text{and} \quad G = \frac{\rho g a^2}{\mu}. \tag{3.11}$$

Here Γ is the ratio of surface-tension forces to elastic forces, T_ℓ is the ratio of longitudinal wall tension to surface-tension, T_0 is the ratio of initial circumferential tension to surface tension, M is the ratio of wall mass to fluid mass and G is the ratio of wall damping to fluid damping. In addition, we define a damping parameter $\phi = \epsilon^3 MG$ which remains finite in the limit $\epsilon \to 0$, so that the following evolution equation for the wall displacement is obtained:

$$\phi\frac{\partial \eta}{\partial t} = T_\ell\frac{\partial^2\eta}{\partial z^2} + T_0\frac{\eta}{1+\epsilon\eta} - \frac{1}{\Gamma}\frac{\eta}{(1+\epsilon\eta)^2} + \frac{\partial^2 h}{\partial z^2} + \frac{h}{(1-\epsilon)(1+\epsilon(h-1))}. \tag{3.12}$$

4. Linear stability analysis

Estimates for the dimensionless parameters appearing in the evolution equations (3.9) and (3.12) are based on the properties and dimensions of the terminal bronchioles of the lungs and the liquid lining. The following dimensional values appropriate for such airways were chosen: $a = 2.5 \times 10^{-2}$ cm, $a-b = 2.25 \times 10^{-3}$ cm, $E = 6 \times 10^4$ dynes/cm^2, $g = 10$ s^{-1}, $h_0 = 2.5 \times 10^{-3}$ cm, $T_\ell = 25$ dynes/cm (based on a pleural pressure of -5 cm H_2O), $\gamma = 0.5$, $\mu = 0.01$ P, $\rho_w = 1$ g/cm^3, $\sigma = 20$ dynes/cm. The dimensionless parameter values based on the above are: $\epsilon = 0.1$, $\phi = 6.25 \times 10^{-5}$, $\Gamma = 0.1$, $T_\ell = 1.25$. A wide range of parameter values will be investigated since there is variability in the dimensions of airways and wall properties can, for example, change with disease. Hence we will consider cases where the film is either thin ($\epsilon \leqslant 0.1$) or thick ($\epsilon = 0.2$), the wall is stiff ($\Gamma \ll 1$) or compliant ($\Gamma = O(1)$) and weakly ($\phi = O(10^{-5})$) or strongly damped ($\phi = O(1)$).

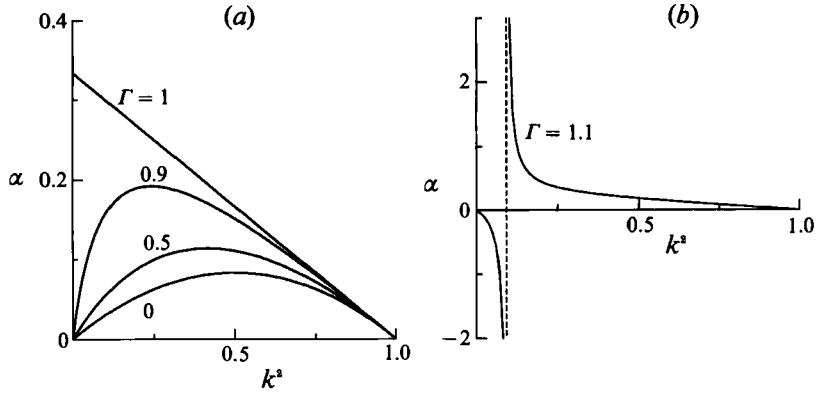

FIGURE 2. α versus k^2 for $\phi = T_\ell = 0$: (*a*) $\Gamma = 0, 0.5, 0.9, 1$; (*b*) $\Gamma = 1.1$.

In this section a linear stability analysis of the evolution equations (3.9) and (3.12) is performed using the method of normal modes. The time evolution of small disturbances of the air–liquid and wall–liquid interfaces are represented by

$$h = h_1 e^{\alpha t + ikz} \quad \text{and} \quad \eta = \eta_1 e^{\alpha t + ikz}, \tag{4.1}$$

where the constant amplitudes of the disturbances, h_1 and η_1, are very small, that is $|h_1| \ll 1$, $|\eta_1| \ll 1$, k is the wavenumber and α is the growth rate. These are substituted into (3.9) and (3.12) to yield the following dispersion relation for α:

$$\chi\phi\alpha^2 + [1 + \chi T_\ell k^2 + \chi(k^2-1)(\tfrac{1}{3}k^2\phi + 1)]\alpha + \tfrac{1}{3}[1 + \chi T_\ell k^2] k^2(k^2-1) = 0, \tag{4.2}$$

where $\chi = \Gamma/(1 - \Gamma T_0)$. Since we are interested in small initial hoop stresses, $\chi > 0$ for $\Gamma > 0$ and small T_0. When $T_0 = 0$, $\chi = \Gamma$. Hence the effect of including $T_0 > 0$ is the same as replacing χ by a larger value of Γ, and therefore is destabilizing since a positive hoop stress tends to collapse the tube. If there is no wall damping, i.e. $\phi = 0$, then

$$\alpha = \frac{k^2(1-k^2)(1+\chi T_\ell k^2)}{3(1+\chi T_\ell k^2 - \chi(1-k^2))}. \tag{4.3}$$

Note that the rigid-tube case is obtained by setting $\chi = 0$. Figure 2(*a*) shows the variation of α with respect to k^2 for various values of $\Gamma \leqslant 1$ with $T_0 = T_\ell = 0$. For $\Gamma < 1$, the system is always unstable if $0 < k^2 < 1$, with h_1 and η_1 being in phase and $h_1/\eta_1 > 1$. The maximum growth rate, $\alpha_{\max}$, increases with increasing Γ, that is with increasing surface tension or decreasing E. Also, the value of k at $\alpha = \alpha_{\max}$ decreases with increasing Γ. Surface tension stabilizes short-wavelength disturbances and consequently $\alpha < 0$ for $k^2 > 1$. In this case h_1 and η_1 are of opposite sign, with $|h_1/\eta_1| > 1$ if $1 < k^2 < 1 + 1/\Gamma$ and $|h_1/\eta_1| < 1$ if $k^2 > 1 + 1/\Gamma$. Figure 2(*a*) also shows that the maximum growth rate occurs at $k = 0$ for $\Gamma = 1$. The behaviour for $\Gamma > 1$ is quite different since the denominator in (4.3) vanishes when $k = k_c = (1 - 1/\Gamma)^{\frac{1}{2}}$, implying that there is an infinite growth rate at a finite wavelength (figure 2*b*). The effect of the longitudinal tension parameter, T_ℓ, is to dampen disturbances and delay the onset of the infinite growth rate to larger wavelengths (figure 3). The critical wavenumber is given by $k_c^2 = (\Gamma - 1)/\Gamma(T_\ell + 1)$.

This singular behaviour disappears if the damping parameter, ϕ, is retained. Then the appropriate solution of (4.2) is given by the positive root

$$2\chi\phi\alpha = [(1 + \chi T_\ell k^2 + \chi(k^2-1)(\tfrac{1}{3}k^2\phi + 1))^2 - \tfrac{4}{3}k^2(k^2-1)(1+\chi T_\ell k^2)\chi\phi]^{\frac{1}{2}} - \chi(k^2-1)(\tfrac{1}{3}k^2\phi + 1) - \chi T_\ell k^2 - 1, \tag{4.4}$$

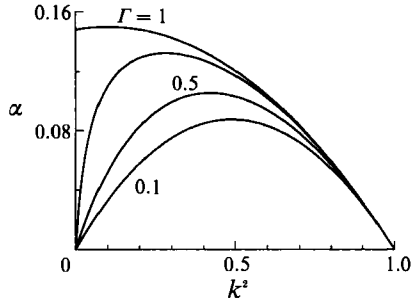

FIGURE 3. α versus k^2 for $\phi = 0$, $T_\ell = 1.25$; $\Gamma = 0.1, 0.5, 0.9, 1$.

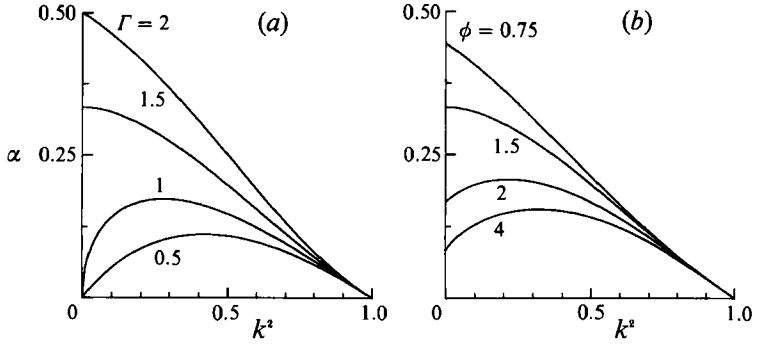

FIGURE 4. α versus k^2 for: (*a*) $\phi = 1$, $T_\ell = 0$ and $\Gamma = 0.5, 1, 1.5, 2$; (*b*) $\Gamma = 1.5$, $T_\ell = 0$ and $\phi = 0.75, 1.5, 2, 4$.

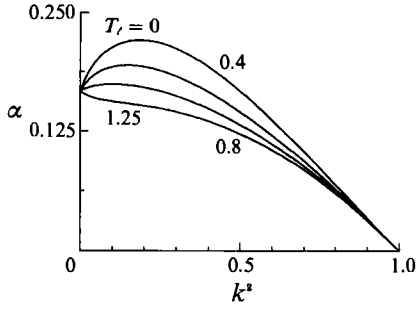

FIGURE 5. α versus k^2 for $\Gamma = 1.2$, $\phi = 1$ and $T_\ell = 0, 0.4, 0.8, 1.25$.

since the other root is never positive for the range of parameter values that are of interest. For all parameter values, we still have an unstable system if $0 \leqslant k < 1$ and a stable one if $k \geqslant 1$. The effect of Γ on α for $\phi = 1$ and $T_\ell = 0$ is shown in figure 4 (*a*). As expected, the maximum growth rate increases with increasing Γ, but in this case there is no infinite growth rate at finite wavenumber. For $\Gamma > 1$, α is non-zero at $k = 0$ and $\alpha_{\max} = (\Gamma - 1)/\Gamma\phi$ at $k = 0$ if $\Gamma \geqslant 3/(3-\phi)$. If there is sufficient damping, $\phi \geqslant 3$, then the maximum growth rate never occurs at $k = 0$. This is displayed in figure 4 (*b*), where ϕ is allowed to vary with $\Gamma = 1.5$ and $T_\ell = 0$. Increasing wall damping leads to smaller $\alpha_{\max}$ and larger $k_{\max}$. The effect of longitudinal tension parameter, T_ℓ, is shown in figure 5 for $\Gamma = 1.2$ and $\phi = 1$. As T_ℓ increases, the growth rate decreases in the interval $0 < k < 1$. If $T_\ell \geqslant \Gamma\phi/3(\Gamma - 1) - 1$, then the maximum growth rate occurs at $k = 0$ and is independent of T_ℓ, $\alpha_{\max} = (\Gamma - 1)/(\Gamma\phi)$ at $k = 0$.

We can conclude that there is capillary instability with some wall motion if the wavenumber of the disturbance is smaller than one. This is the same result as found by Rayleigh (1902) for the rigid-tube case. For very compliant airways with $\Gamma \geqslant 3/(3-\phi)$ and $\phi < 3$, the fastest growth rate occurs at $k = 0$ implying that these airways uniformly shut down. This is referred to as compliant collapse by Kamm & Schroter (1989). Wall damping and longitudinal wall tension have stabilizing effects on film disturbances and if $\phi \geqslant 3$ there is no compliant collapse.

5. Nonlinear stability

Equations (3.9) and (3.12) are solved numerically using the method of lines (Holt 1984). A system of ordinary differential equations is obtained by replacing the z-derivatives with fourth-order finite differences and solved using Gear's method. As in Hammond (1983) and Gauglitz & Radke (1988), periodic boundary conditions were prescribed, so that odd derivatives with respect to z vanish:

$$\frac{\partial^{2j+1}h}{\partial z^{2j+1}} = \frac{\partial^{2j+1}\eta}{\partial z^{2j+1}} = 0 \quad \text{for} \quad j = 0, 1, 2, \ldots \quad \text{at} \quad z = 0, \tfrac{1}{2}L, \tag{5.1}$$

where L is the wavelength of the initial disturbances, and

$$h(z,0) = A\cos(2\pi z/L), \qquad \eta(z,0) = B\cos(2\pi z/L). \tag{5.2a, b}$$

In Hammond's thin-film analysis, using a rigorously derived asymptotic approximation (i.e. (3.9) with $\epsilon = 0$), disturbances grew with time, but reached quasi-steady states consisting of a series of lobes whose number depended on L. Gauglitz & Radke (1988) solved (3.9) for the rigid wall case ($\eta = 0$ for all time) with the above initial condition (5.2a). They showed that the growth of the initial disturbances depended critically on the initial thickness and wavelength. For a given L there is a value of ϵ for which the minimum core radius, $r_{\min} = 1 + \epsilon(h-1)$, tends to zero in finite time, i.e. a liquid bridge forms. The lubrication theory approximation becomes invalid when this occurs, but Johnson *et al.* (1991) have shown that their one-dimensional model is a good approximation until just before meniscus formation, and therefore is accurate in predicting when closure occurs. Computations were stopped before $r_{\min} = 0$ and before the magnitude of the inertia terms neglected in (3.4), estimated using the numerically computed solutions, became $O(1)$. In all cases, the leading-order axial viscous term and pressure gradient were several orders of magnitude larger than the neglected inertial terms, and only in the very late stages just prior to closure, when the film becomes thick and fluid is accelerated into the growing lobe, did inertia become important.

Figure 6 shows the time evolution of both wall–liquid and air–liquid interfaces for $\Gamma = 0.1$, $\phi = 1$, $\epsilon = 0.1$, $T_\ell = 0$, $L/a = 2.866\pi$. The value of L/a chosen here is the most dangerous wavelength based on linear stability theory. This ratio is kept fixed, except in the case where the variation in length is investigated. Initially both interfaces are out of phase, but after a short while they become in phase as predicted by linear theory. As the perturbations grow, the film becomes flat and thin at $2z/L \approx 1$ where the two interfaces approach each other, and there is little fluid motion here except where the air–liquid interface curves away from the wall. With time, the length of the flattened region increases since fluid flows into the growing lobe located at $z = 0$. The pressure inside the growing lobe is approximately constant and consequently the location of the wall near $z = 0$ is independent of z. The film becomes very thin, of the order of 1 μm, where the two interfaces curve away from each other

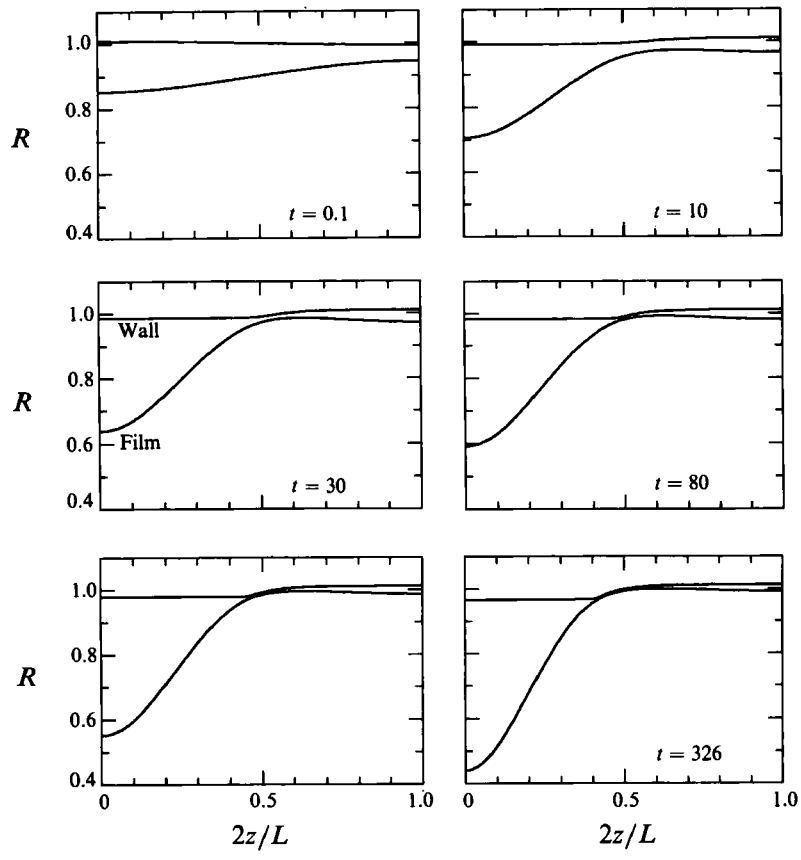

FIGURE 6. Air–liquid, $1+\epsilon(h(z,t)-1)$, and wall–liquid, $1+\epsilon\eta(z,t)$, interfaces plotted as functions of z at $t = 0.1$, 10, 30, 80, 163, 326. $\Gamma = 0.1$, $\phi = 1$, $\epsilon = 0.1$, $T_\ell = 0$, $L/a = 2.866\pi$.

at $2z/L \approx 0.5$. The air–liquid interface is displaced radially inward by the wall motion and this reduces its radius of curvature, implying that wall flexibility promotes greater instability. For the parameter values chosen in figure 6 meniscus formation occurs at $t \approx 330$. In figure 7, Γ is increased compared to figure 6. If we consider the increase on the basis of smaller E and fixed σ then the timescales are the same in both figures. The effect of larger Γ is to promote faster meniscus formation since the minimum core radius reaches the position $r \approx 0.42$ at $t = 3.75$ when $\Gamma = 0.5$ (figure 7) and at $t = 326$ when $\Gamma = 0.1$ (figure 6). From the development of the disturbance, clearly the more flexible case allows for greater deflection radially, thus reducing the minimum core radius by wall motion. Another effect, however, is that the narrowest portion of the liquid layer in figure 7, just prior to closure, is much thicker than that of figure 6 just prior to closure. Hence, the draining of liquid into the meniscus experiences significantly more shear resistance when Γ is smaller and contributes to the larger time taken for the bulge at $z = 0$ to reach a critical volume and become unstable.

As in Gauglitz & Radke (1988), there is a critical value of $\epsilon = \epsilon_c$ such that $r_{\min} \to 0$ as $t \to t_c$. This value is unique for a fixed-wavelength disturbance which we choose as twice the airway length. For a liquid-lined flexible tube, ϵ_e is a function of both fluid and wall properties. For example, the dependence of ϵ_c on Γ is shown in figure 8 for fixed wavelength and two values of ϕ corresponding to a strongly damped

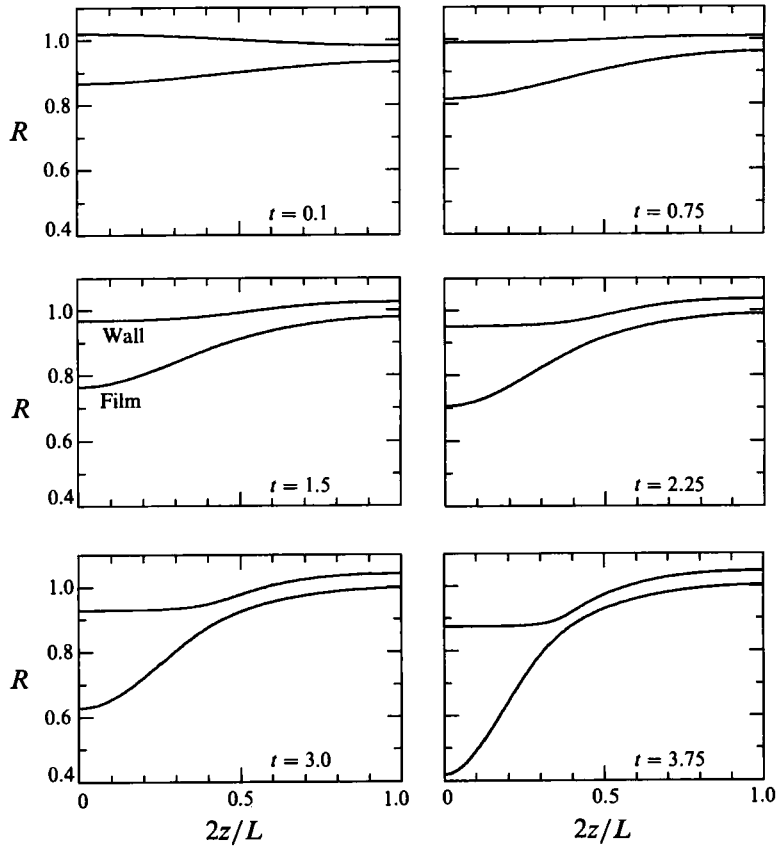

FIGURE 7. Air–liquid, $1+\epsilon(h(z,t)-1)$, and wall–liquid, $1+\epsilon\eta(z,t)$, interfaces plotted as functions of z at $t = 0.1, 0.75, 1.5, 2.25, 3, 3.75$. $\Gamma = 0.5$, $\phi = 1$, $\epsilon = 0.1$, $T_\ell = 0$, $L/a = 2.866\pi$.

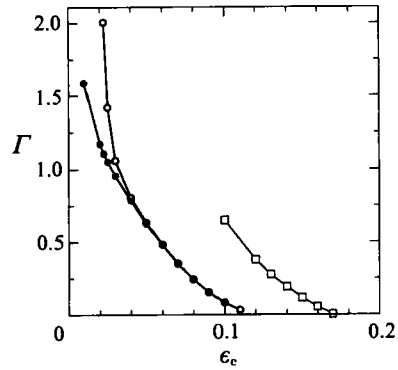

FIGURE 8. Γ versus ϵ_c for ○, $\phi = 1$, $T_\ell = 0$, $L/a = 2.866\pi$; ●, $\phi = 6.25\times10^{-5}$, $T_\ell = 0$, $L/a = 2.866\pi$; □, $\phi = 5\times10^{-4}$, $T_\ell = 1.25$, $L/a = 6$.

system ($\phi = 1$) and weakly damped system ($\phi = 6.25\times10^{-5}$). The dimensional closure time is chosen to be no more than 10 s. As expected, the critical initial film thickness, ϵ_c, decreases with increasing wall flexibility, i.e. increasing Γ. This is physically reasonable since the destabilizing force in this problem is the transverse radius of curvature of the air–liquid interface. When the wall deflects inward it is affecting this radius of curvature in a manner similar to a thicker liquid lining. The

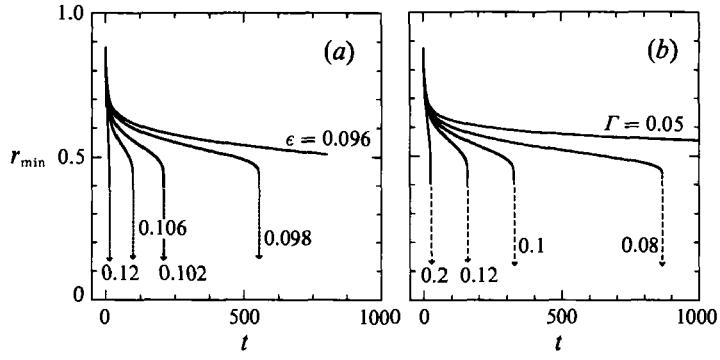

FIGURE 9. $1+\epsilon(h(0,t)-1)$ versus t for: (a) $\epsilon = 0.096$, 0.098, 0.102, 0.106, 0.12; (b) $\Gamma = 0.05$, 0.08, 0.1, 0.12, 0.2.

thicker film has the added effect of allowing the meniscus to grow faster since opposing shear stresses in the thin neck region are smaller. Decreasing ϕ has a stronger effect at larger values of Γ resulting in smaller values of ϵ_c.

In figure 9(a), the minimum core radius, r_{min}, is plotted versus time for various values of ϵ. For sufficiently small ϵ, disturbances tend to quasi-steady solutions consisting of constant-pressure lobes and thin straight segments, similar to the results of Hammond (1983) for the rigid-tube problem. For $\epsilon \geqslant 0.098$ and $t < 600$, disturbances initially grow exponentially as predicted by linear stability theory, but instead of saturating they grow rapidly ($r_{min} \to k_1(t_c - t)^{\xi}$ as $t \to t_c$ with $0 < \xi < 1$) when the film is sufficiently thick, and a meniscus forms after finite time. If ϵ is 20% or more larger than ϵ_c then the long period of time during which r_{min} decreases very slowly disappears since the lobe at $z = 0$ reaches a critical volume before the film becomes very thin and the shear resistance becomes very large. This phenomenon is consistent with results obtained by Johnson *et al.* (1991) and Otis *et al.* (1990) for larger ϵ. In figure 9(b), Γ is varied as the minimum core radius is plotted versus time. If Γ is sufficiently small ($\Gamma = 0.05$), meniscus formation does not occur since there is not sufficient wall motion or the capillary forces are too small. As explained before, a decrease in E leads to greater wall motion inducing faster meniscus formation and therefore closure time decreases with increasing Γ for fixed σ. Γ can also be increased by increasing σ, but σ affects the timescale by a factor of σ^{-1} (3.3). A liquid bridge forms at $t \approx 330$ for $\Gamma = 0.1$ and at $t \approx 900$ for $\Gamma = 0.08$. Hence faster meniscus formation can also occur by increasing σ since in this situation a 25% increase in σ leads to a reduction of closure time by approximately two thirds.

The closure time, t_c^*, is plotted as a function of Γ for $\phi = 1$ and $\phi = 5 \times 10^{-4}$ in figure 10(a). For $\phi = 1$, closure time decreases by a couple of orders of magnitude as a result of increased wall flexibility, from $\Gamma = 0.1$ to $\Gamma = 2$. The value of $t_c^*/(\mu a/\sigma)$ decreases very rapidly for $\Gamma < 0.25$ and is independent of Γ for $\Gamma \geqslant 1$. If $\Gamma \geqslant 1$, t_c^* is independent of Γ for fixed σ. This is because when the tube is sufficiently floppy the radially inward motion of both air–liquid and liquid–wall interfaces is extremely rapid. However, if Γ is doubled from one to two due to a doubling in σ, t_c^* is halved. This is a result of capillary instability only. For small Γ, $0 \leqslant \Gamma \leqslant 0.25$, t_c^* grows asymptotically as $\Gamma \to 0$. Meniscus formation takes an infinitely long time for the rigid-tube limit since the value of ϵ chosen here is smaller than the critical value for the rigid tube. Also, the closure time is independent of wall damping for $\Gamma < 0.2$ because the tube is relatively stiff and consequently there is not much wall motion. In this range of Γ closure is due to capillary instability only. However, for a weakly

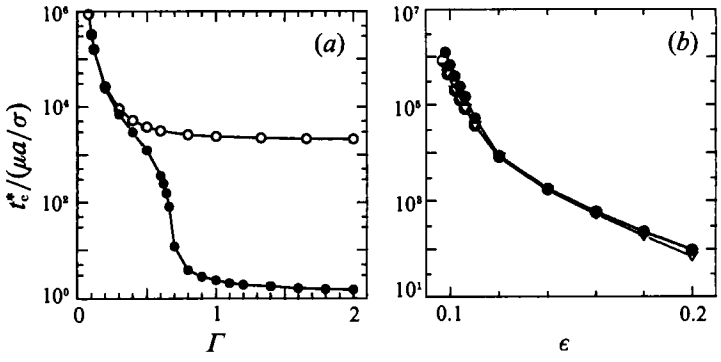

FIGURE 10. (*a*) Closure time versus Γ for ○, $\phi = 1$; ●, $\phi = 5 \times 10^{-4}$, with $\epsilon = 0.1$, $T_\ell = 0$, $L/a = 2.866\pi$. (*b*) Closure time versus ϵ with $\Gamma = 0.1$, $L/a = 2.866\pi$ and ○, $T_\ell = 0$, $\phi = 1$; ●, $T_\ell = 1.25$, $\phi = 1$; ▽, $T_\ell = 0$, $\phi = 6.25 \times 10^{-5}$.

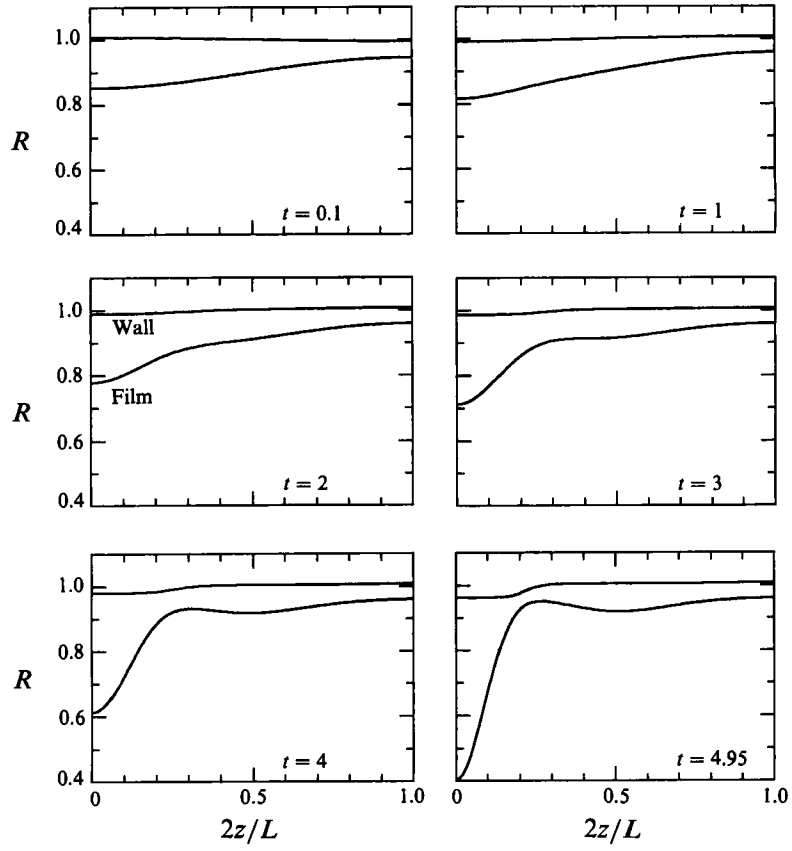

FIGURE 11. Air–liquid, $1+\epsilon(h(z,t)-1)$, and wall–liquid, $1+\epsilon\eta(z,t)$, interfaces plotted as functions of z at $t = 0.1$, 1, 2, 3, 4, 4.95. $\Gamma = 0.1$, $\phi = 1$, $\epsilon = 0.1$, $T_\ell = 0$, $L/a = 6\pi$.

damped system ($\phi = 5 \times 10^{-4}$), closure occurs much more rapidly for $\Gamma > 0.2$ since for floppier tubes there is hardly any force preventing the walls from collapsing. This transition is very rapid: t_c^* drops by three orders of magnitude as Γ increases from 0.5 to 0.8. In figure 10(*b*) t_c^* is plotted versus ϵ. As can be seen, $t_c^*/(\mu a/\sigma)$ decreases monotonically by four orders of magnitude as ϵ increases from 0.097 to 0.2; for $\epsilon = 0.1$, $t_c^* \approx 10.4$ s and for $\epsilon = 0.2$, $t_c^* \approx 0.0012$ s. Longitudinal tension and wall damping

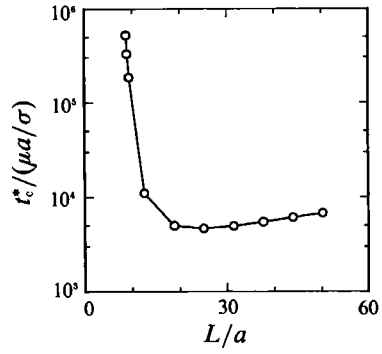

FIGURE 12. Closure time t_c^* versus L/a with $\Gamma = 0.1$, $T_\ell = 0$, $\epsilon = 0.1$ and $\phi = 1$.

do not have much effect on closure time. An increase in T_ℓ leads to longer t_c^* only as $\epsilon \to 0$ and a decrease in ϕ leads to shorter t_c^* as the film becomes relatively thick initially.

The effect of varying wavelength is also investigated. In figure 11, L/a is increased to 6π, and the film thickness does not become as small as in figure 6 before meniscus formation. In addition, as observed by Hammond (1983), a secondary lobe is formed because the film breaks up into constant-pressure lobes on either side of the thinning region. In figure 12, t_c^* is plotted as a function of L/a and shows that for fixed ϵ there is a critical wavelength which minimizes t_c^*. For $\Gamma = 0.1$, $\phi = 1$, $\epsilon = 0.1$, $T_\ell = 0$, the critical value is about twice that predicted by linear stability and the minimum t_c^* is about one order of magnitude smaller than the case when the most dangerous wavelength is given by linear theory.

5.1. *Applications to the lung*

The above model can be applied to airway closure since the airways of the lungs are liquid-lined flexible tubes which are tethered to the lung parenchyma. As in Elad, Kamm & Shapiro (1988*b*), the tethering effect of the parenchyma can be lumped together with the properties of the airway walls. They derive an empirical pressure–area tube law appropriate for airways which is given by

$$\Delta P = K(\beta^n - 1) = K(\eta)\,((1+\epsilon\eta)^{2n} - 1), \tag{5.3}$$

where β is the dimensionless cross-sectional area, n is a coefficient dependent on wall properties and K is an effective wall stiffness parameter which depends nonlinearly on volume change. This term has a similar effect to the term multiplying Γ^{-1} in (3.12). Hence Γ^{-1} can be thought of an effective stiffness parameter combining the effects of wall stiffness and parenchymal stiffness, and the inclusion of wall tethering can be incorporated by considering a thicker-walled tube which has the effect of reducing Γ.

Johnson *et al.* (1991) and Otis *et al.* (1990) used their numerical analysis of rigid-tube models which included fluid inertia to calculate the time taken for a sinusoidal perturbation of the air–liquid interface to occlude the lumen of an airway. The airway length-to-radius ratio was chosen to be 6, which is appropriate for generation-15 airways (Weibel 1963), with the wavelength of the initial disturbance equal to the airway length and $\epsilon = 0.2$. Johnson *et al.* (1991) obtained $t_c^* \approx 0.065$ s using both their small-ϵ and arbitrary-film-thickness models. Using $A = 0.001$ and $B = 0$ for the amplitudes of the initial disturbances in (5.2), we obtained a value of $t_c^* \approx 0.06$ s, which agrees well with theirs, when we set $\Gamma = 0$. For the flexible-airway case using typical wall parameters, $T_\ell = 1.25$, $\phi = 5 \times 10^{-4}$ and $\Gamma = 0.1$, $t_c^* \approx 0.045$ s, i.e. a 25%

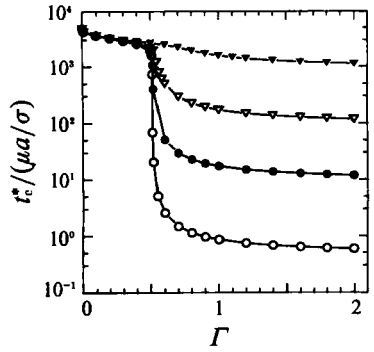

FIGURE 13. Closure time versus Γ for ○, $\phi = 5 \times 10^{-4}$; ●, $\phi = 0.01$; ▽, $\phi = 0.1$; ▼, $\phi = 1$ with $\epsilon = 0.2$, $T_\ell = 1.25$ and $L/a = 6$.

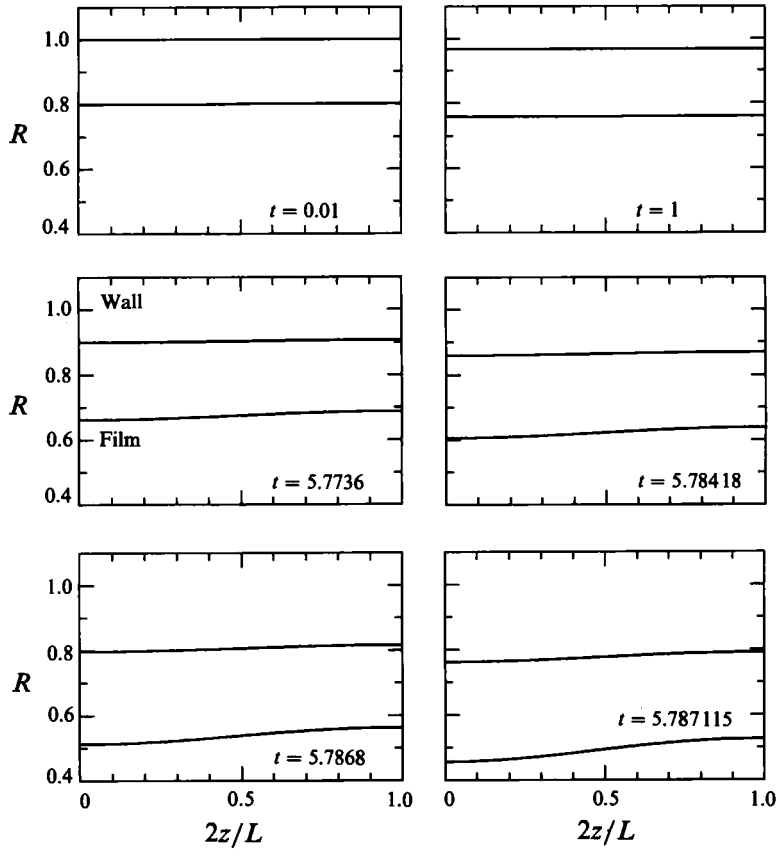

FIGURE 14. Air–liquid, $1+\epsilon(h(z,t)-1)$, and wall–liquid, $1+\epsilon\eta(z,t)$, interfaces plotted as functions of z at $t = 0.01$, 1, 5.7736, 5.78418, 5.7868, 5.787115 with $\Gamma = 0.514$, $\phi = 5 \times 10^{-4}$, $T_\ell = 1.25$, $\epsilon = 0.2$ and $L/a = 6$.

reduction compared to the rigid-tube case. Figure 8 also shows how Γ varies with ϵ_c for $T_\ell = 1.25$, $\phi = 5 \times 10^{-4}$ and $L/a = 6$. For this set of parameters, $\epsilon_c(\Gamma = 0) \approx 0.172$, $\epsilon_c(\Gamma = 0.1) \approx 0.152$ and $\epsilon_c(\Gamma = 0.5) \approx 0.109$, which clearly demonstrates that the volume of fluid in the liquid lining required for closure strongly depends on wall and fluid properties even for relatively stiff airways. In figure 13, $t_c^*/(\mu a/\sigma)$ is plotted versus Γ for various values of ϕ. As explained before, for small Γ the closure time is

independent of ϕ because there is no significant wall motion. At $\Gamma \approx 0.5$, a decrease in wall damping leads to more rapid closure, implying that there is a transition from surface-tension-driven instability to compliant collapse. A case corresponding to rapid airway closure, $\Gamma = 0.514$, $\phi = 5 \times 10^{-4}$, $\epsilon = 0.2$, $T_\ell = 1.25$, $L/a = 6$, is shown in figure 14. Initially there is hardly any fluid motion and therefore the air–liquid and liquid–wall interfaces are pulled inward and almost parallel to each other. When the radius of curvature is approximately 0.5, collapse is very rapid and occurs at $t \approx 5.787$ (i.e. $t_c^* \approx 0.0091$ s, which is approximately 85% faster than the corresponding rigid-tube case).

6. Conclusions

We have modelled the linear and nonlinear dynamics of a thin film consisting of a Newtonian fluid coating a thin flexible circular tube. This model attempts to characterize the relevant physical parameters which promote the closure of the small airways of the lungs either by the meniscus formation or wall collapse, and represents a first step towards more realistic models which will incorporate non-axisymmetric disturbances to mimic non-circular airway collapse.

Nonlinear evolution equations for the air–liquid and wall–liquid interfaces are derived from first principles. Lubrication theory is used since the film thickness is small compared to the length of an airway and fluid inertia is negligible except in the very final stages of collapse (Johnson *et al.* 1991). As in the models proposed by Gauglitz & Radke (1988) and Johnson *et al.* (1991), a more accurate expression for the interfacial curvature is employed than that used by Hammond (1983), which contains terms that become large as the film thickens. In the long-wavelength limit, a simple wall model can be used where only radial displacements are considered.

The results presented in this paper demonstrate that there are two important mechanisms which promote airway closure: meniscus formation and compliant collapse. These instabilities strongly depend on ϵ, the initial non-dimensionalized film thickness, Γ, the ratio of surface-tension to elastic forces, and L, the wavelength of the disturbance. Linear stability theory shows that if Γ is sufficiently small then there is a capillary instability for $L/a > \pi$. Otherwise, if $\Gamma \geqslant 3/(3-\phi)$ and $\phi < 3$, the most unstable mode is compliant collapse. For airways this occurs when $\Gamma \geqslant 1$ since $\phi \ll 1$. A nonlinear theory is employed to estimate the time it takes for a meniscus to form and show the dependency of the critical initial film thickness, ϵ_c, on the flexibility parameter Γ. Figure 9(*a*) indicates that an increase in ϵ leads to faster closure times, t_c^*, which is consistent with results for rigid tubes (Gauglitz & Radke 1988) and that there can be up to three timescales depending on the size of ϵ. Initially, for very small ϵ, the minimum core radius decays exponentially as predicted by linear stability theory, and is followed by a period in which decay is very slow since flow resistance increases dramatically as the film becomes extremely thin. Eventually sufficient fluid is accumulated in the growing lobe to induce rapid meniscus formation. This phenomenon is not observed for large ϵ (Johnson *et al.* 1991; Otis *et al.* 1990). Figure 10(*b*) also shows that constant longitudinal tension and wall damping do not have a significant effect on closure times for small Γ. An increase in Γ due to smaller Young's modulus also induces smaller closure times, and smaller ϵ_c values are required for closure. Figure 8 demonstrates that ϵ_c strongly depends on wall and fluid properties, for example $\epsilon_c(\Gamma = 0.1)/\epsilon_c(\Gamma = 0) \approx 0.75$–$0.88$ and $\epsilon_c(\Gamma = 0.5)/\epsilon_c(\Gamma = 0) \approx 0.5$–$0.65$. Hence closure can be greatly enhanced in diseases where Γ has a value above normal. Figures 10(*a*) and 13 indicate that closure time is

independent of wall flexibility if there is sufficient wall damping. For weakly damped systems, there is a rapid transition between closure due to capillary effects and due to wall collapse at approximately $\Gamma = 0.5$, which is half the value obtained using linear stability theory. The discrepancy may be because the linear theory does not take into the account the thickness of the unperturbed film. An example of coupled capillary–compliant instability is shown in figure 14 for $\Gamma = 0.514$ and $\epsilon = 0.2$.

Another interesting result is that the most dangerous wavelength (or fastest growing mode) computed using the nonlinear model is longer than that predicted by linear stability theory (figure 12).

Understanding the effects of initial film thickness, surface tension of the air–liquid interface and modulus of elasticity of the wall on meniscus formation and compliant collapse could be of great importance in recognizing certain respiratory diseases. These two possible mechanisms for airway closure may be relevant in: (i) respiratory distress syndrome of premature neonates which is due to an abnormally high surface tension of the lung's liquid lining and an inability of the lungs to produce surfactant; (ii) in emphysema, where the elastance of the airways can become small enough and the thickness of the liquid lining may be abnormally high; (ii) in asthma, which is sometimes accompanied by airway mucosal and luminal edema and therefore an increase in lung fluid.

This research was funded by NIH grants K04-HL01818, R01-HL41126 and NSF grant CTS-9013083, as well as a supercomputing grant from the Pittsburgh Supercomputing Center, Pittsburgh, PA, through the NIH Division of Research cooperative agreement U41 RR04154.

REFERENCES

ATABEK, H. B. & LEW, H. S. 1966 Wave propagation through a viscous incompressible fluid contained in an initially stressed elastic tube. *Biophys. J.* **6**, 481–503.

CRAWFORD, A. B. H., COTTON, D. J., PAIVA, M. & ENGEL, L. A. 1989 Effect of airway closure on ventilation distribution. *J. Appl. Physiol.* **66**, 2511–2515.

DRAGON, C. A. & GROTBERG, J. B. 1991 Oscillatory flow and mass transport in a flexible tube. *J. Fluid Mech.* **231**, 135–155.

ELAD, D., FOUX, A. & KIVITY, Y. 1988*a* A model for the nonlinear elastic response of large arteries. *J. Biomed. Engng* **110**, 185–189.

ELAD, D., KAMM, R. D. & SHAPIRO, A. H. 1988*b* Tube law for the intrapulmonary airway. *J. Appl. Physiol.* **65**, 7–13.

FRAZER, D. G., WEBER, K. C. & FRANZ, G. N. 1985 Evidence of sequential opening and closing of lung units during inflation–deflation of excised rat lungs. *Resp. Physiol.* **61**, 277–288.

GAUGLITZ, P. A. & RADKE, C. J. 1988 An extended evolution equation for liquid film breakup in cylindrical capillaries. *Chem. Engng Sci.* **43**, 1457–1465.

GOLDENVEIZER, A. C. 1961 *Theory of Elastic Thin Shells.* Pergamon.

GOREN, S. L. 1962 The instability of an annular thread of fluid. *J. Fluid Mech.* **12**, 309–319.

HAMMOND, P. S. 1983 Nonlinear adjustment of a thin annular film of viscous fluid surrounding a thread of another within a circular pipe. *J. Fluid Mech.* **137**, 363–384.

HICKOX, C. 1971 Instability due to a viscosity and density stratification in axisymmetric pipe flow. *Phys. Fluids* **14**, 251–262.

HOLT, M. 1984 *Numerical Method in Fluid Dynamics.* Springer.

HUGHES, J. M. B., ROSENZWEIG, D. Y. & KIVITZ, P. B. 1970 Site of airway closure in excised dog lungs: histologic demonstration. *J. Appl. Physiol.* **29**, 340–344.

JOHNSON, M., KAMM, R., HO, L. W., SHAPIRO, A. & PEDLEY, T. J. 1991 The nonlinear growth of surface-tension-driven instabilities of a thin annular film. *J. Fluid Mech.* **223**, 141–156.

KAMM, R. D. & JOHNSON, M. 1990 Airway closure at low lung volume: The role of liquid film instabilities. *Appl. Mech. Rev.* **43**, Part 2, S92–97.

KAMM, R. D. & SCHROTER, R. C. 1989 Is airway closure caused by a thin liquid instability? *Respir. Physiol.* **75**, 141–156.

MACKLEM, P. T., PROCTOR, D. F. & HOGG, J. C. 1970 The stability of peripheral airways. *Respir, Physiol.* **8**, 191–203.

ORON, A. & ROSENAU, P. 1989 Nonlinear evolution and breaking of interfacial Rayleigh–Taylor waves. *Phys. Fluids* A **1**, 1155–1165.

OTIS, D. R., JOHNSON, M., PEDLEY, T. J. & KAMM, R. D. 1990 The effect of surfactant on liquid film stability in the peripheral airways. Abstract, ASME Winter Annual Meeting.

RAYLEIGH, LORD 1902 On the instability of cylindrical fluid surfaces. In *Scientific Papers*, vol. 3, pp. 594–996. Cambridge University Press.

ROSENAU, P. & ORON, A. 1989 Evolution and breaking of liquid film flowing on a vertical cylinder. *Phys. Fluids* A **1**, 1763–1766.

WEIBEL, E. R. 1963 *Morphometry of the Human Lung*. Academic.